

Prospective evaluation of a portable depth-sensitive optical spectroscopy device to identify oral neoplasia

Richard A. Schwarz,¹ Wen Gao,¹ Vanda M. T. Stepanek,² Tao T. Le,²
Vijayashree S. Bhattar,² Michelle D. Williams,³ Jessica K. Wu,⁴
Nadarajah Vigneswaran,⁴ Karen Adler-Storthz,⁴ Ann M. Gillenwater,²
and Rebecca Richards-Kortum^{1,*}

¹Department of Bioengineering, Rice University, 6100 Main Street, Houston, TX 77005, USA

²Department of Head and Neck Surgery, University of Texas M. D. Anderson Cancer Center,
1515 Holcombe Boulevard, Houston, TX 77030, USA

³Department of Pathology, University of Texas M. D. Anderson Cancer Center, 1515 Holcombe Boulevard, Houston,
TX 77030, USA

⁴University of Texas Dental Branch at Houston, 6516 M. D. Anderson Boulevard, Houston, TX 77030, USA
*rkortum@rice.edu

Abstract: A portable, depth-sensitive clinical spectroscopy device for noninvasive early diagnosis of oral cancer is described. We carried out a pilot study to evaluate the ability of the device to identify oral neoplasia using a previously developed diagnostic algorithm. A total of 79 oral sites in 33 subjects, including 28 patients with oral lesions and 5 healthy volunteers, were measured and analyzed. Measurements of 54 nonkeratinized oral sites yielded an area under the receiver operating characteristic curve of 0.90. Measurements of 25 keratinized oral sites yielded an area under the receiver operating characteristic curve of 0.83.

©2010 Optical Society of America

OCIS codes: (170.6510) Spectroscopy, tissue diagnostics; (170.3890) Medical optics instrumentation.

References and links

1. B. W. Stewart, and P. Kleihues, eds., *World Cancer Report* (IARC, 2003), Chap. 5.
2. S. F. Altekruse, C. L. Kosary, M. Krapcho, N. Neyman, R. Aminou, W. Waldron, J. Ruhl, N. Howlander, Z. Tatalovich, H. Cho, A. Mariotto, M. P. Eisner, D. R. Lewis, K. Cronin, H. S. Chen, E. J. Feuer, D. G. Stinchcomb, and B. K. Edwards, eds., *SEER Cancer Statistics Review, 1975–2007* (National Cancer Institute, Bethesda, MD, http://seer.cancer.gov/csr/1975_2007/, based on November 2009 SEER data submission, posted to the SEER web site, 2010).
3. A. D. Ravidis, P. Gullane, J. D. Langdon, J. L. Lefebvre, C. Scully, and J. P. Shah, "Major advances in the knowledge and understanding of the epidemiology, aetiopathogenesis, diagnosis, management and prognosis of oral cancer," *Oral Oncol.* **45**(4-5), 299–300 (2009).
4. D. M. Laronde, T. G. Hislop, J. M. Elwood, and M. P. Rosin, "Oral cancer: just the facts," *J. Can. Dent. Assoc.* **74**(3), 269–272 (2008).
5. M. P. Rethman, W. Carpenter, E. E. W. Cohen, J. Epstein, C. A. Evans, C. M. Flaitz, F. J. Graham, P. P. Hujuel, J. R. Kalmar, W. M. Koch, P. M. Lambert, M. W. Lingen, B. W. Oettmeier, Jr., L. L. Patton, D. Perkins, B. C. Reid, J. J. Sciubba, S. L. Tomar, A. D. Wyatt, Jr., K. Aravamudhan, J. Frantsve-Hawley, J. L. Cleveland, D. M. Meyer; American Dental Association Council on Scientific Affairs Expert Panel on Screening for Oral Squamous Cell Carcinomas, "Evidence-based clinical recommendations regarding screening for oral squamous cell carcinomas," *J. Am. Dent. Assoc.* **141**(5), 509–520 (2010).
6. J. A. Yellowitz, A. M. Horowitz, T. F. Drury, and H. S. Goodman, "Survey of U.S. dentists' knowledge and opinions about oral pharyngeal cancer," *J. Am. Dent. Assoc.* **131**(5), 653–661 (2000).
7. A. Ariyawardana, and L. Ekanayake, "Screening for oral cancer/pre-cancer: knowledge and opinions of dentists employed in the public sector dental services of Sri Lanka," *Asian Pac. J. Cancer Prev.* **9**(4), 615–618 (2008).
8. E. Applebaum, T. N. Ruhlen, F. R. Kronenberg, C. Hayes, and E. S. Peters, "Oral cancer knowledge, attitudes and practices: a survey of dentists and primary care physicians in Massachusetts," *J. Am. Dent. Assoc.* **140**(4), 461–467 (2009).
9. P. E. Petersen, "Oral cancer prevention and control--the approach of the World Health Organization," *Oral Oncol.* **45**(4-5), 454–460 (2009).
10. S. Fedele, "Diagnostic aids in the screening of oral cancer," *Head Neck Oncol* **1**(1), 5 (2009).

11. L. L. Patton, J. B. Epstein, and A. R. Kerr, "Adjunctive techniques for oral cancer examination and lesion diagnosis: a systematic review of the literature," *J. Am. Dent. Assoc.* **139**(7), 896–905, quiz 993–994 (2008).
12. M. W. Lingen, J. R. Kalmar, T. Karrison, and P. M. Speight, "Critical evaluation of diagnostic aids for the detection of oral cancer," *Oral Oncol.* **44**(1), 10–22 (2008).
13. I. J. Bigio, and S. G. Bown, "Spectroscopic sensing of cancer and cancer therapy: current status of translational research," *Cancer Biol. Ther.* **3**(3), 259–267 (2004).
14. M. G. Müller, T. A. Valdez, I. Georgakoudi, V. Backman, C. Fuentes, S. Kabani, N. Laver, Z. Wang, C. W. Boone, R. R. Dasari, S. M. Shapshay, and M. S. Feld, "Spectroscopic detection and evaluation of morphologic and biochemical changes in early human oral carcinoma," *Cancer* **97**(7), 1681–1692 (2003).
15. D. C. G. de Veld, M. Skurichina, M. J. H. Witjes, R. P. W. Duin, H. J. C. M. Sterenborg, and J. L. N. Roodenburg, "Autofluorescence and diffuse reflectance spectroscopy for oral oncology," *Lasers Surg. Med.* **36**(5), 356–364 (2005).
16. A. Gillenwater, V. Papadimitrakopoulou, and R. Richards-Kortum, "Oral premalignancy: new methods of detection and treatment," *Curr. Oncol. Rep.* **8**(2), 146–154 (2006).
17. P. M. Lane, T. Gilhuly, P. Whitehead, H. Zeng, C. F. Poh, S. Ng, P. M. Williams, L. Zhang, M. P. Rosin, and C. E. MacAulay, "Simple device for the direct visualization of oral-cavity tissue fluorescence," *J. Biomed. Opt.* **11**(2), 024006 (2006).
18. I. Pavlova, M. Williams, A. El-Naggar, R. Richards-Kortum, and A. Gillenwater, "Understanding the biological basis of autofluorescence imaging for oral cancer detection: high-resolution fluorescence microscopy in viable tissue," *Clin. Cancer Res.* **14**(8), 2396–2404 (2008).
19. V. R. Kolli, H. E. Savage, T. J. Yao, and S. P. Schantz, "Native cellular fluorescence of neoplastic upper aerodigestive mucosa," *Arch. Otolaryngol. Head Neck Surg.* **121**(11), 1287–1292 (1995).
20. J. K. Dhingra, D. F. Perrault, Jr., K. McMillan, E. E. Rebeiz, S. Kabani, R. Manoharan, I. Itzkan, M. S. Feld, and S. M. Shapshay, "Early diagnosis of upper aerodigestive tract cancer by autofluorescence," *Arch. Otolaryngol. Head Neck Surg.* **122**(11), 1181–1186 (1996).
21. C. S. Betz, M. Mehlmann, K. Rick, H. Stepp, G. Grevers, R. Baumgartner, and A. Leunig, "Autofluorescence imaging and spectroscopy of normal and malignant mucosa in patients with head and neck cancer," *Lasers Surg. Med.* **25**(4), 323–334 (1999).
22. D. L. Heintzelman, U. Utzinger, H. Fuchs, A. Zuluaga, K. Gossage, A. M. Gillenwater, R. Jacob, B. Kemp, and R. R. Richards-Kortum, "Optimal excitation wavelengths for *in vivo* detection of oral neoplasia using fluorescence spectroscopy," *Photochem. Photobiol.* **72**(1), 103–113 (2000).
23. S. McGee, J. Mirkovic, V. Mardirossian, A. Elackattu, C. C. Yu, S. Kabani, G. Gallagher, R. Pistey, L. Galindo, K. Badizadegan, Z. Wang, R. Dasari, M. S. Feld, and G. Grillone, "Model-based spectroscopic analysis of the oral cavity: impact of anatomy," *J. Biomed. Opt.* **13**(6), 064034 (2008).
24. D. C. G. De Veld, M. J. H. Witjes, H. J. C. M. Sterenborg, and J. L. N. Roodenburg, "The status of *in vivo* autofluorescence spectroscopy and imaging for oral oncology," *Oral Oncol.* **41**(2), 117–131 (2005).
25. A. Amelink, O. P. Kaspers, H. J. C. M. Sterenborg, J. E. van der Wal, J. L. N. Roodenburg, and M. J. H. Witjes, "Non-invasive measurement of the morphology and physiology of oral mucosa by use of optical spectroscopy," *Oral Oncol.* **44**(1), 65–71 (2008).
26. L. T. Nieman, C. W. Kan, A. Gillenwater, M. K. Markey, and K. Sokolov, "Probing local tissue changes in the oral cavity for early detection of cancer using oblique polarized reflectance spectroscopy: a pilot clinical trial," *J. Biomed. Opt.* **13**(2), 024011 (2008).
27. S. McGee, V. Mardirossian, A. Elackattu, J. Mirkovic, R. Pistey, G. Gallagher, S. Kabani, C. C. Yu, Z. Wang, K. Badizadegan, G. Grillone, and M. S. Feld, "Anatomy-based algorithms for detecting oral cancer using reflectance and fluorescence spectroscopy," *Ann. Otol. Rhinol. Laryngol.* **118**(11), 817–826 (2009).
28. S. K. Majumder, A. Gupta, S. Gupta, N. Ghosh, and P. K. Gupta, "Multi-class classification algorithm for optical diagnosis of oral cancer," *J. Photochem. Photobiol. B* **85**(2), 109–117 (2006).
29. R. A. Schwarz, D. Arifler, S. K. Chang, I. Pavlova, I. A. Hussain, V. Mack, B. Knight, R. Richards-Kortum, and A. M. Gillenwater, "Ball lens coupled fiber-optic probe for depth-resolved spectroscopy of epithelial tissue," *Opt. Lett.* **30**(10), 1159–1161 (2005).
30. R. A. Schwarz, W. Gao, D. Daye, M. D. Williams, R. Richards-Kortum, and A. M. Gillenwater, "Autofluorescence and diffuse reflectance spectroscopy of oral epithelial tissue using a depth-sensitive fiber-optic probe," *Appl. Opt.* **47**(6), 825–834 (2008).
31. R. A. Schwarz, W. Gao, C. Redden Weber, C. Kurachi, J. J. Lee, A. K. El-Naggar, R. Richards-Kortum, and A. M. Gillenwater, "Noninvasive evaluation of oral lesions using depth-sensitive optical spectroscopy," *Cancer* **115**(8), 1669–1679 (2009).
32. I. van der Waal, "Potentially malignant disorders of the oral and oropharyngeal mucosa; terminology, classification and present concepts of management," *Oral Oncol.* **45**(4-5), 317–323 (2009).
33. P. M. Speight, "Update on oral epithelial dysplasia and progression to cancer," *Head Neck Pathol.* **1**(1), 61–66 (2007).
34. I. Pavlova, C. R. Weber, R. A. Schwarz, M. D. Williams, A. M. Gillenwater, and R. Richards-Kortum, "Fluorescence spectroscopy of oral tissue: Monte Carlo modeling with site-specific tissue properties," *J. Biomed. Opt.* **14**(1), 014009 (2009).
35. K. Huff, P. C. Stark, and L. W. Solomon, "Sensitivity of direct tissue fluorescence visualization in screening for oral premalignant lesions in general practice," *Gen. Dent.* **57**(1), 34–38 (2009).

1. Introduction

Approximately 390,000 new cases of oral cancer and oropharyngeal cancer occur worldwide each year, of which about two-thirds are in developing nations [1]. In the United States an estimated 161,000 men and 88,000 women are currently living with a diagnosis of cancer of the oral cavity or pharynx, and the overall five-year survival rate for patients with the disease is 61% [2]. Major advances have been made in basic treatment methods including surgery, radiotherapy and chemotherapy [3]. However, early diagnosis remains critically important. The five-year survival rate in the United States is 83% for oral cancer patients diagnosed when the cancer is localized, 55% when it has spread to regional lymph nodes, and 32% when it has metastasized; but only one-third of patients are diagnosed at the early, localized stage [2].

Risk factors for oral and oropharyngeal cancer include the use of tobacco, alcohol, betel quid, areca nut, and paan, increased age, immunological compromise, unhealthy diet, and infection with the human papilloma virus [4]. Opportunistic screening for oral cancer typically occurs through visual and tactile examination of the oral cavity by a dental or medical professional, or other health care worker during a general examination. An expert panel of the American Dental Association Council recommends that clinicians remain alert for signs of potentially malignant lesions while performing routine dental examinations, especially in patients who are at high risk due to tobacco or alcohol use; however, the panel cautions that there is not yet sufficient evidence to determine whether routine screening of asymptomatic patients actually reduces mortality due to oral cancer [5]. Furthermore, while awareness of the importance of oral cancer screening is increasing, surveys indicate that a significant fraction of dentists and physicians do not consider themselves adequately trained to perform screening procedures [6–8]. Low-cost, robust diagnostic aids that can be implemented in low-resource settings are needed, as well as further studies on the predictive power of population-based oral cancer screening [9].

Adjunctive techniques for early detection and diagnosis of oral cancer include brush biopsy, toluidine blue staining, chemiluminescence, optical imaging, and optical spectroscopy [10]. While some of these diagnostic aids show promise, none has yet been definitively proven to perform better than conventional visual examination [11,12]. The accepted method for diagnosis of oral cancer and potentially malignant lesions remains clinical examination and histopathological evaluation of biopsied tissue [5].

Optical spectroscopy is a noninvasive diagnostic method that has been investigated in many forms including fluorescence spectroscopy, elastic or diffuse scattering spectroscopy, and Raman spectroscopy [13]. Spectroscopic measurements can detect biochemical and architectural alterations in tissue that are related to the progression of precancer and therefore provide diagnostic information [13–15]. These alterations may include changes in the concentrations of native fluorophores such as collagen, elastin, keratin, nicotinamide adenine dinucleotide (NADH), and flavin adenine dinucleotide (FAD); changes in hemoglobin concentration and oxygenation; increasing epithelial thickness; and increasing nuclear size and nuclear/cytoplasmic ratio [16–18].

Investigations of autofluorescence spectroscopy of oral lesions *in vivo* have identified differences among the emission spectra of normal, premalignant and malignant tissues at excitation wavelengths in the ultraviolet and visible region [19–22]. Considerable success has been reported in distinguishing lesions from healthy oral mucosa, but the spectral variations among different anatomic sites within the oral cavity and the problem of discriminating benign lesions from precancerous/cancerous lesions continue to pose challenges [23,24]. Recent investigations reflect these complexities, including measurement techniques that target localized, superficial tissue regions where early premalignant changes are believed to occur [25,26]; algorithms that are explicitly based on specific anatomic sites within the oral cavity [27]; and multi-class algorithms that are designed to classify tissue into a range of diagnostic categories [28].

We previously developed a fiber optic probe capable of interrogating specific depth regions in tissue [29] and incorporated it into a clinical spectroscopy device [30]. We carried out a clinical study of depth-sensitive optical spectroscopy [31] to identify the most diagnostically useful illumination wavelengths and to develop an algorithm for diagnostic classification of nonkeratinized oral tissue. While these results showed good sensitivity and specificity, the device was not easily portable and was therefore not well suited for community-based health care settings. Here we describe a compact, portable version of the depth-sensitive optical spectroscopy device that is designed to measure only the most diagnostically useful parameters. The portable device was evaluated through measurements of 79 oral sites in 33 subjects, including 28 patients with oral lesions and 5 healthy volunteers.

2. Methods

2.1 Instrumentation

The portable depth-sensitive spectroscopy device is shown in Fig. 1. It is 36 cm x 20 cm x 25 cm in size and weighs 6.3 kg. Light-emitting diodes (LEDs) are used for illumination. Two LEDs are used for fluorescence excitation: part #NCSU034A (Nichia Corporation, Tokushima, Japan, 310 mW at 500 mA, peak wavelength 385 nm). A 385-nm bandpass filter with a spectral full width of 11 nm (Semrock, Inc., Rochester, New York) is placed in each fluorescence excitation pathway. Two LEDs are used for reflectance illumination: Vio High Power White LED part #GE-VHD-1A-3C7 (GE Lumination, East Cleveland, Ohio, 180 lumens at 350 mA). A 320-nm longpass filter (Edmund Optics Inc., Barrington, New Jersey) is placed in each reflectance illumination pathway. Light is delivered and collected via a ball-lens coupled fiber optic probe that is placed in contact with the tissue. The probe contains two depth channels: a shallow depth channel designed to target the epithelium (a depth region from approximately 0 μm – 400 μm), and a medium depth channel designed to target the epithelium and shallow stroma (a depth region from approximately 0 μm – 900 μm). The probe is identical to a previously described depth-sensitive probe [30] except that the illumination and collection fibers for the two deep channels have been omitted in the current probe. Collected light is delivered through a 405-nm longpass filter (Chroma Technology Corp., Rockingham, Vermont) to a miniature spectrometer (USB2000 + , Ocean Optics, Inc., Dunedin, Florida). Light sources and optical filters are dedicated to their respective measurement channels and there are no moving parts. Automated data acquisition, real-time processing and diagnostic classification are controlled by a laptop computer using LabVIEW software (National Instruments Corporation, Austin, Texas) for instrumentation control and MATLAB software (The MathWorks, Inc., Natick, Massachusetts) for data analysis. The total cost of components, including the depth-sensitive probe and the laptop computer, is less than 10,000 USD.

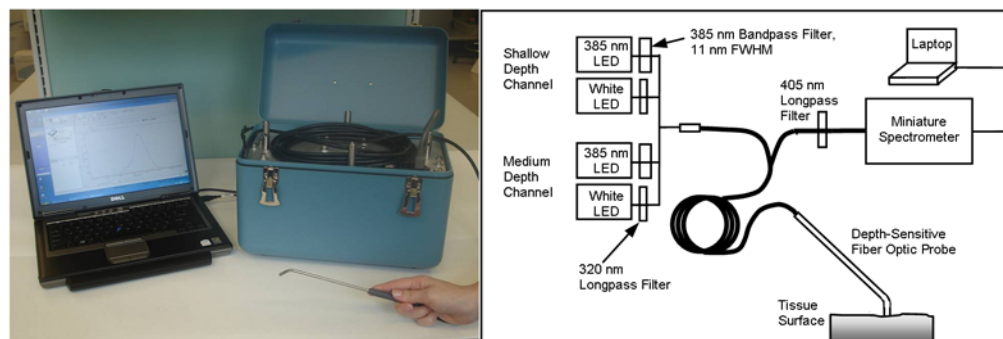


Fig. 1. Photograph and diagram of the portable depth-sensitive optical spectroscopy device.

Fluorescence spectra and diffuse reflectance spectra are collected through each of the two depth channels. Fluorescence spectra are collected using 385 nm excitation (11 nm full width

at half maximum) and reflectance spectra are collected using white light illumination. The device collects four spectra per measurement: fluorescence measured in the medium depth channel (FM), fluorescence measured in the shallow depth channel (FS), reflectance measured in the medium depth channel (RM), and reflectance measured in the shallow depth channel (RS). Optical power is adjusted independently in each channel such that the detected signal level is in an optimal range (high signal to noise ratio, but not near saturation). The optical power delivered to the tissue in each case is 155 μ W (FM), 155 μ W (FS), 3.5 μ W (RM) and 5.5 μ W (RS). A background spectrum is also collected with no illumination. The use of a limited set of depth channels and illumination wavelengths enables compact design and rapid data acquisition, while still allowing depth selectivity and measurement of key features. Each spectrum is collected with an integration time of 500 ms and the total time required for a complete measurement is 5 seconds.

2.2 Human subjects

The study was conducted at the University of Texas M. D. Anderson Cancer Center (MDACC). The study was approved by the Institutional Review Boards at MDACC and Rice University. Patients with lesions of the oral mucosa and healthy volunteers 18 years or older were recruited to participate. Written informed consent was obtained from all subjects.

2.3 Measurement procedure

Spectroscopic measurements of patients were performed in the operating room at MDACC immediately prior to surgery (26 patients) or in the Head & Neck clinic (2 patients). The oral cavity was first inspected visually. Several sites in each subject were selected for spectroscopic measurement, including at least one oral lesion and at least one contralateral site with a normal clinical appearance. The clinical appearance of each measured site, as judged by an expert observer, was recorded and categorized as normal, abnormal low risk for neoplasia, abnormal high risk for neoplasia, or cancer. The probe was placed gently in contact with the site and held in place by the clinician for two successive measurements. Measurements were performed in a darkened room to minimize the effects of ambient light.

Upon completion of the optical measurements 4-mm punch biopsies were collected from one abnormal-appearing measurement site and one normal-appearing contralateral measurement site. Specimens were placed in fixative and submitted for histopathologic evaluation. Histopathology diagnoses were categorized as normal/benign, mild dysplasia, moderate/severe dysplasia, or cancer using standard diagnostic criteria [32,33]. Normal/benign was defined as normal, hyperkeratosis, hyperplasia, and/or inflammation without dysplasia or with only focal mild dysplasia; there were no benign tumors in the study. In this group of 28 patients, measurement sites without a corresponding biopsy to serve as the gold standard were excluded from the analysis.

Measurements of five healthy volunteers were performed in an examination room at MDACC. In healthy volunteers biopsies were not performed but the clinical appearance of measured sites was noted.

Optical calibration standards were measured daily before or after patient measurements. Calibration standards included two positive fluorescence standards (Rhodamine B in ethylene glycol, 2 mg/L and 8 g/L); two negative fluorescence standards (frosted surface of a quartz cuvette and deionized ultrafiltered water); and a positive reflectance standard (Teflon). The spectrum of a calibrated tungsten halogen light source (Ocean Optics, Inc.) was measured and used to correct for nonuniform spectral variations in the throughput of the detection system.

2.4 Data analysis

Data processing and analysis consisted of the following steps: (1) processing of spectroscopic data to yield calibrated reflectance and fluorescence spectra, (2) extraction of quantitative optical features required for the classification algorithm, (3) application of the classification algorithm to calculate the posterior probability of disease, and (4) application of a threshold value to generate a diagnostic prediction. The prior probability of disease was set to 0.50.

Procedures for data processing have been previously described [30], including background subtraction, correction for illumination energy, correction for system throughput, and (for reflectance data) calculation of the ratio of tissue reflectance to the reflectance of a white Teflon standard. FM, FS, and RS spectra measured with the portable device were used directly as processed. A multiplicative correction factor was applied to the processed RM spectra to account for inter-instrument differences between the portable device and the instrument that was originally used to develop the algorithm; these differences were associated with probe-to-probe variations in stray light reflected from the ball lens surfaces within the probe tip. This inter-instrument correction factor was developed from healthy volunteer data and standards data collected prior to the clinical study reported here.

The classification algorithm used in this study has been previously described [31]. It is a two-class linear discriminant analysis-based classifier that was developed for nonkeratinized oral tissue in a previous clinical study. The algorithm generates a posterior probability and a diagnostic prediction based on features of the autofluorescence and reflectance spectra. The algorithm uses six spectral features as input values for classification: (1) 472 nm fluorescence emission intensity at 385 nm excitation, medium depth channel; (2) ratio of reflectance intensity at 650 nm to reflectance intensity at 500 nm, medium depth channel; (3) ratio of reflectance intensity at 500 nm to reflectance intensity at 420 nm, medium depth channel; (4) reflectance intensity at 500 nm, medium depth channel; (5) ratio of 478 nm fluorescence emission intensity to 458 nm fluorescence emission intensity at 385 nm excitation, medium depth channel; and (6) reflectance intensity at 420 nm, shallow depth channel.

Nonkeratinized oral sites in the current data set were classified using the original classification algorithm and threshold value for posterior probability (0.55) without modification. Keratinized oral sites in the current data set were classified using the same classification algorithm, but for keratinized tissue the threshold value was optimized retrospectively to 0.94 to maximize the sum of the sensitivity and specificity. Processing and classification were done in real time such that the fully processed spectra, the posterior probability value, and the diagnostic prediction were available immediately after the completion of the measurement. The higher posterior probability value resulting from two measurements at a given site was used as the posterior probability value for that site.

For sites in patients, the histopathology result from the biopsy taken at the measurement site was used as the gold standard. Histopathology diagnoses of normal/benign or mild dysplasia were considered non-neoplastic; diagnoses of moderate/severe dysplasia or cancer were considered neoplastic. For healthy volunteers, expert clinical impression was used as the gold standard since no biopsies were collected.

Sensitivity, specificity, positive predictive value, and negative predictive value were calculated on a per-site basis with respect to the gold standard. Confidence intervals were calculated using the Clopper-Pearson method.

3. Results

During the 8-month period from November 2009 to June 2010, 264 measurements were collected from 135 sites in 29 patients, and 48 measurements were collected from 24 sites in 5 healthy volunteers. All measurements passed a quality control check. Histopathology results from a corresponding biopsy were available for 110 measurements in 55 sites in 28 patients; all of these measurements were included in the analysis. All measurements in healthy volunteers were included in the analysis. The final data set consisted of 158 measurements from 79 sites in 33 subjects, as shown in Table 1.

Of the 79 sites in the data set, 54 sites were at anatomic locations categorized here as nonkeratinized, including lateral tongue (24), buccal mucosa (13), floor of mouth (9), and ventral tongue (8). There were 25 sites at anatomic locations categorized as keratinized, including gingiva (15), hard palate (7), mandible (2) and dorsal tongue (1).

Table 1. Number of Subjects, Sites, and Measurements

		Patients	Healthy Volunteers	Total
Data set	Subjects	28	5	33
	Sites	55	24	79
	Measurements	110	48	158
Subset: Nonkeratinized tissue	Subjects represented ^a	21	5	26
	Sites	40	14	54
	Measurements	80	28	108
Subset: Keratinized tissue	Subjects represented ^a	9	5	14
	Sites	15	10	25
	Measurements	30	20	50

^aSome subjects are represented in both the nonkeratinized subset and the keratinized subset.

Table 2 shows the expert clinical impression and the corresponding histopathologic diagnosis for sites in patients. Of the 55 sites in patients, 29 were non-neoplastic (normal/benign or mild dysplasia) and 26 were neoplastic (moderate/severe dysplasia or cancer) according to histopathology. The 24 sites in healthy volunteers were all considered non-neoplastic based on clinical impression, including one site described as abnormal low risk due to inflammation.

Table 2. Clinical Impression vs. Histopathology for Sites in Patients

Histopathology Diagnosis	Expert Clinical Diagnosis				Total Sites
	Normal	Abnormal Low Risk	Abnormal High Risk	Cancer	
Normal/benign	23	1	0	0	24
Mild dysplasia	2	0	2	1	5
Moderate/severe dysplasia	0	0	3	2	5
Cancer	0	1	1	19	21
Total sites	25	2	6	22	55

Figure 2 shows average spectra collected from nonkeratinized sites (108 spectra from 54 sites) broken down by diagnosis. Plots are shown for fluorescence medium depth, fluorescence shallow depth, reflectance medium depth, and reflectance shallow depth configurations. These plots suggest that for nonkeratinized tissue, the spectral characteristics of neoplastic sites (moderate/severe dysplasia or cancer, shown in red) are distinct from those of non-neoplastic sites (normal or mild dysplasia, shown in blue). The most striking characteristic of the spectra shown in Fig. 2 is the substantial decrease in blue-green autofluorescence of neoplastic tissue compared to non-neoplastic tissue, observed in both the medium and shallow depth channels. A decrease in the intensity of the reflectance spectra from neoplastic tissue is also observed in both the medium and shallow depth channels.

In addition to intensity differences, small shape differences may be noted in the average spectra. The average reflectance spectra from cancer sites display a slightly deeper valley at 420 nm relative to 500 nm than the average reflectance spectra from normal sites. The average fluorescence spectra from neoplastic sites display a small peak at 635 nm, associated with porphyrin fluorescence, that is not present in the spectra from non-neoplastic sites.

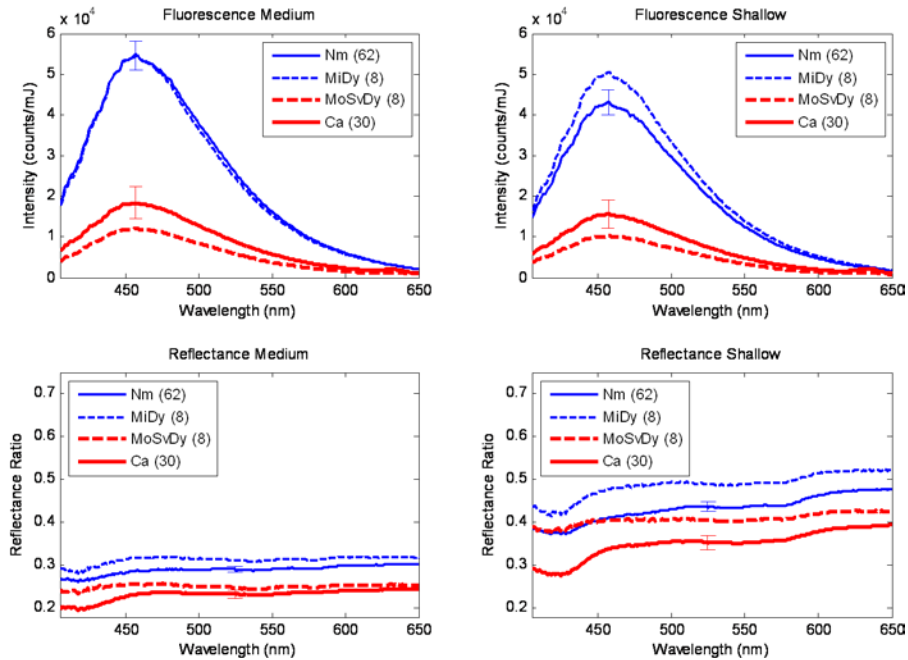


Fig. 2. Average spectra of nonkeratinized oral sites. Nm: Normal. MiDy: Mild Dysplasia. MoSvDy: Moderate/Severe Dysplasia. Ca: Cancer. Number in parentheses indicates number of spectra represented in the average. Error bars, shown only for categories with >10 spectra, indicate standard error of the mean.

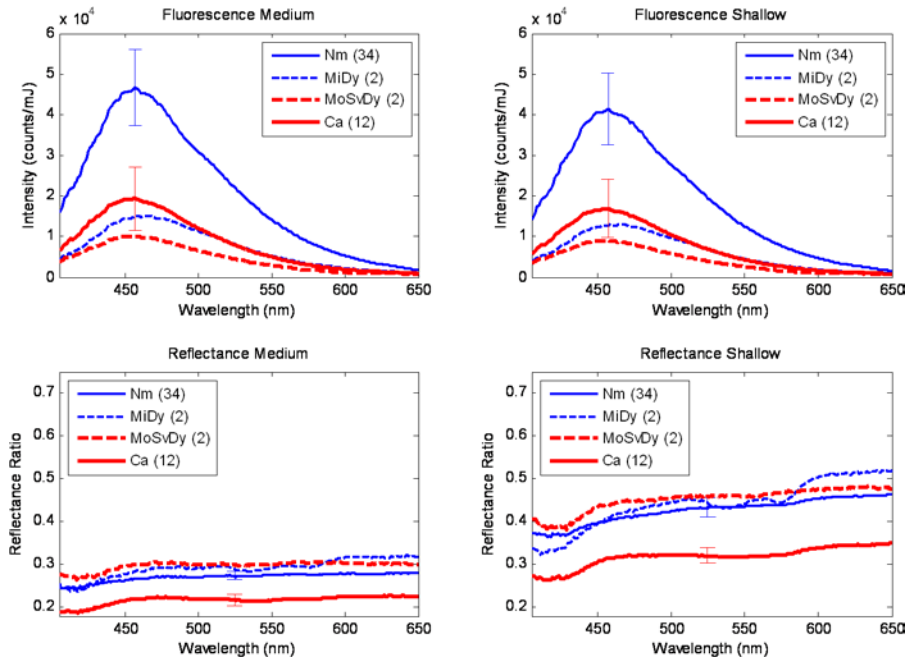


Fig. 3. Average spectra of keratinized oral sites. Nm: Normal. MiDy: Mild Dysplasia. MoSvDy: Moderate/Severe Dysplasia. Ca: Cancer. Number in parentheses indicates number of spectra represented in the average. Error bars, shown only for categories with >10 spectra, indicate standard error of the mean.

Figure 3 shows average spectra collected from keratinized sites (50 spectra from 25 sites) in the same format. Greater variability is observed in the fluorescence spectra for keratinized tissue, indicated by the larger error bars in Fig. 3 compared to Fig. 2. Despite this greater variability, the same overall trends of reduced fluorescence intensity and reduced reflectance intensity are observed in cancer sites relative to normal sites.

Table 3 summarizes the sensitivity, specificity, positive predictive value, and negative predictive value obtained in this study using the portable device. Figure 4 shows the corresponding receiver operating characteristic (ROC) curves. For nonkeratinized sites the area under the ROC curve was 0.90. At the point indicated on the ROC curve, corresponding to a preestablished threshold value, sensitivity was 84% (16/19) and specificity was 91% (32/35). The preestablished threshold was very close to the optimal value (Q-point) on the ROC curve for nonkeratinized sites. For keratinized sites the area under the ROC curve was 0.83. At the point indicated on the ROC curve, corresponding to a retrospectively established threshold, sensitivity was 86% (6/7) and specificity was 83% (15/18).

Of the 79 sites in the data set, 6 sites were misclassified as false positive and 4 sites were misclassified as false negative. Sites misclassified as false positive included tongue (2), floor of mouth (1), and gingiva (3). Three of the false positive sites were in patients, including two normal sites and one site with mild dysplasia according to histopathology; the other three sites were in healthy volunteers. Sites misclassified as false negative included buccal mucosa (1), tongue (1), floor of mouth (1), and gingiva (1). All of the false negative sites were cancer according to histopathology.

The relationship between inflammation and diagnostic performance was examined. The presence or absence of inflammation at each measurement site was determined by histopathology (for sites in patients) or by clinical impression (for sites in healthy volunteers). Chronic and/or acute inflammation was present in 28% of the non-neoplastic sites and in 96% of the neoplastic sites in the study. Of the 6 non-neoplastic sites misclassified as false positive, 3 sites (50%) had inflammation present. Of the 4 neoplastic sites misclassified as false negative, 4 sites (100%) had inflammation present.

Table 3. Diagnostic Performance of the Portable Spectroscopy Device^a

	Nonkeratinized Tissue	Keratinized Tissue
Sensitivity	0.84 (0.60, 0.97)	0.86 (0.42, 0.996)
Specificity	0.91 (0.77, 0.98)	0.83 (0.59, 0.96)
Positive predictive value	0.84 (0.60, 0.97)	0.67 (0.30, 0.93)
Negative predictive value	0.91 (0.77, 0.98)	0.94 (0.70, 0.998)

^a95% confidence intervals are shown in parentheses.

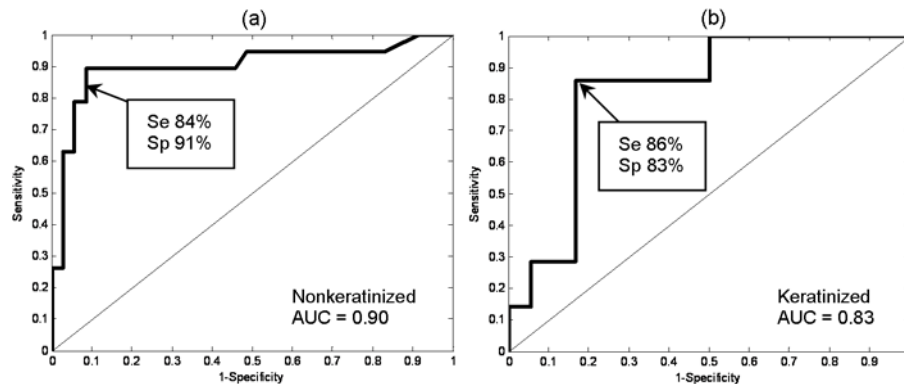


Fig. 4. Receiver operating characteristic curves for (a) nonkeratinized sites and (b) keratinized sites. Arrow in (a) corresponds to a preestablished threshold; arrow in (b) corresponds to a retrospectively established threshold. Se: sensitivity. Sp: specificity. AUC: Area under curve.

4. Discussion

Many groups have reported the development of methods for diagnostic classification of oral tissue based on autofluorescence and/or diffuse reflectance spectroscopy. Müller et al reported a sensitivity of 96% and a specificity of 96% for distinguishing cancerous/dysplastic tissue from normal tissue in a study of 23 subjects [14]. De Veld et al obtained areas under the ROC curve up to 0.90 for distinguishing lesions from healthy oral mucosa in a study of 225 subjects [15]. McGee et al reported areas under the ROC curve of 0.81-0.97 for distinguishing lesions from healthy mucosa, and 0.60-0.75 for distinguishing benign from dysplastic/malignant lesions, in a study of 71 patients [27].

Results are often reported within the data set used to develop the diagnostic classification technique, with or without cross-validation. Studies that apply a previously developed diagnostic algorithm to an independent validation set are less frequent. In a recent study of 124 subjects we developed a diagnostic algorithm for nonkeratinized tissue and applied it to both the training set and an independent validation set [31]. We obtained a sensitivity and specificity of 94% and 90%, respectively, in the training set and 82% and 87%, respectively, in the validation set. Here we report the successful application of that same algorithm to a validation data set that is not only independent, but was in fact collected using a different instrument – a much smaller, portable version of the device.

Of the six spectral features used by the algorithm, spectral feature #1 captures the decrease in blue-green autofluorescence intensity, believed to be primarily due to the breakdown of collagen crosslinks in the shallow stroma, that occurs in neoplastic tissue. Spectral feature #2 characterizes changes in the slope of the reflectance spectrum that occur as increased nuclear size and crowding lead to an increase in scattering in the epithelium relative to the shallow stroma, and as angiogenesis leads to increased hemoglobin absorption in the stroma. Spectral features #3, #4, and #6 are associated with changes in hemoglobin absorption due to the growth of new blood vessels. Spectral feature #5 identifies changes in shape of the fluorescence spectrum due to alterations in the contributions from NADH, FAD and keratin in the epithelium, and a reduced contribution from collagen in the stroma. The algorithm does not use porphyrin fluorescence in the 635-nm wavelength region as a diagnostic feature; this fluorescence is frequently observed in neoplastic tissue but in the training set it was not found to be a sufficiently reliable diagnostic predictor. The relationship between biological alterations and spectral characteristics is explored in detail elsewhere [34].

The current study confirms previous results indicating spectral differences between healthy and diseased tissue. Neoplasia appears to be associated with a decrease in blue-green fluorescence intensity. The classification algorithm uses this change in fluorescence intensity, measured in the medium depth channel (spectral feature #1), as the primary feature for diagnostic prediction. Sites with strong fluorescence intensity in the medium depth channel are usually classified as negative by the algorithm, while sites with loss of fluorescence in the medium depth channel are typically classified as positive. Alterations in the shape and intensity of the reflectance spectra (spectral features #2, #3, #4, #6) and in the shape of the fluorescence peak (spectral feature #5) also affect the diagnostic prediction.

As in previous studies, spectral differences were also observed between nonkeratinized and keratinized oral sites. Keratinized sites in the oral cavity, such as the gingiva and hard palate, are characterized by a protective keratin layer in the superficial epithelium and dense connective tissue in the stroma. Like other oral sites, neoplastic keratinized sites typically display a decrease in blue-green autofluorescence due to the breakdown of collagen crosslinks and increased hemoglobin absorption due to angiogenesis. However, the superficial layer of keratin is variable in thickness and can be highly scattering, providing a variable amount of shielding of collagen and other subsurface fluorophores from optical interrogation. The keratin layer is also itself fluorescent, with a blue fluorescence peak under ultraviolet illumination. In this study greater variability in fluorescence intensity was observed in keratinized tissue than in nonkeratinized tissue, and keratinized sites proved more difficult to classify.

Furthermore, in keratinized tissue we observed that normal-appearing sites in healthy volunteers typically had moderate to low fluorescence intensity, while histologically normal sites in patients tended to have substantially higher fluorescence intensity (Fig. 5b). This makes classification of keratinized sites in a mixed population of patients and healthy volunteers more challenging. One contributing factor to this difference between healthy volunteers and patients may have been that gingival sites in healthy volunteers were typically located adjacent to teeth, while teeth were often missing at the corresponding sites in patients. The difference was much less evident in nonkeratinized tissue (Fig. 5a). Despite these issues, the diagnostic algorithm proved to be sufficiently robust for use with both nonkeratinized and keratinized tissue.

It is believed that the presence of inflammation can be a potential source of false positive results for diagnostic methods based on tissue autofluorescence [35]. The design of the depth-sensitive probe is intended to minimize this effect by interrogating the epithelium and minimizing the signal from the stroma. In this study three of the six false positive non-neoplastic sites (50%) were found to have inflammation present. This percentage was higher than the fraction of all non-neoplastic sites which had inflammation present (28%). Based on this very small sample of sites, inflammation may have been a contributing factor but not the dominant factor in the false positive results obtained in this study.

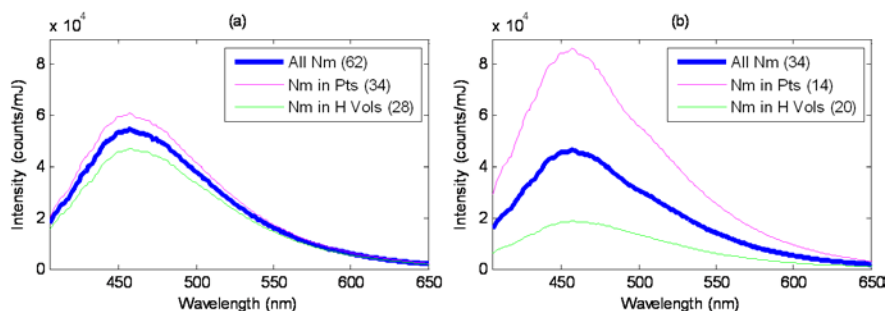


Fig. 5. Average fluorescence spectra of normal oral sites, measured using the medium depth channel, in (a) nonkeratinized tissue and (b) keratinized tissue. All Nm: All normal sites. Nm in Pts: Normal sites in patients only. Nm in H Vols: Normal sites in healthy volunteers only. Number in parentheses indicates number of spectra represented in the average.

The portable spectroscopy device has proven to be well suited for clinical use due to its compact size and its rapid measurement capability. The device is rugged and can be easily transported between clinical sites without the need for optical realignment. Measurements are performed in a darkened room; however, the system performs well even in the presence of a low level of ambient light, which is useful in many clinical situations. We typically perform two successive 5-second measurements at each site; by verifying that the two sets of spectra are consistent, the operator can ensure that no patient movement or probe slippage occurred during the measurement.

In summary, the diagnostic performance of a portable depth-sensitive spectroscopy device was evaluated in a clinical study involving 33 subjects. A previously developed classification algorithm was implemented to classify measured sites. Sensitivity and specificity were 84% and 91%, respectively, for nonkeratinized sites using a preestablished threshold. Sensitivity and specificity were 86% and 83%, respectively, for keratinized sites using a retrospectively established threshold. The development of portable clinical instrumentation and the implementation of algorithms for real-time diagnostic prediction should facilitate the translation of optical spectroscopy to community and low-resource settings where it can be used to aid in early diagnosis of oral cancer.

Acknowledgments

This research was supported by National Cancer Institute grant number R01CA095604.